Calculation of complex DNA damage induced by ions

Eugene Surdutovich,[1,2] David C. Gallagher,[1] and Andrey V. Solov'yov[2,*]
[1]*Department of Physics, Oakland University, Rochester, Michigan 48309, USA*
[2]*Frankfurt Institute for Advanced Studies, Ruth-Moufang-Strasse 1, D-60438 Frankfurt am Main, Germany*
(Received 9 July 2011; revised manuscript received 23 October 2011; published 23 November 2011)

This paper is devoted to the analysis of the complex damage of DNA irradiated by ions. The assessment of complex damage is important because cells in which it occurs are less likely to survive because the DNA repair mechanisms may not be sufficiently effective. We study the flux of secondary electrons through the surface of nucleosomes and calculate the radial dose and the distribution of clustered damage around the ion's path. The calculated radial dose distribution is compared to simulations. The radial distribution of the complex damage is found to be different from that of the dose. A comparison with experiments may solve the question of what is more lethal for the cell, damage complexity or absorbed energy. We suggest a way to calculate the probability of cell death based on the complexity of the damage. This work is done within the framework of the phenomenon-based multiscale approach to radiation damage by ions.

DOI: 10.1103/PhysRevE.84.051918 PACS number(s): 87.53.−j, 81.40.Wx, 61.80.−x, 41.75.Ak

I. INTRODUCTION: MULTISCALE APPROACH TO RADIATION DAMAGE

Ion-beam cancer therapy has recently been in a stage of booming development. Despite the success of this technique, a number of scientific questions on the microscopic level have not yet been resolved. This field has attracted much attention in the scientific community [1–9]. Among the studies is the multiscale approach to the radiation damage induced by irradiation with ions, aimed at the phenomenon-based quantitative understanding of the scenario from the incidence of an energetic ion on tissue to the cell death. This approach combines many spatial, temporal, and energetic scales involved in this scenario. The success of this approach will provide a phenomenon-based foundation for ion-beam cancer therapy, radiation protection in space, and other applications of ion beams. The main issues addressed by the multiscale approach are ion stopping in the medium [10]; the production and transport of secondary electrons produced as a result of ionization and excitation of the medium [10,11]; the interaction of secondary particles with biological molecules, the most important being DNA [7]; the analysis of induced damage; and the evaluation of the probabilities of subsequent cell survival or death. This approach is interdisciplinary since it is based on physics, chemistry, and biology. Moreover, it spans several areas within each of these disciplines.

The multiscale approach started with the analysis of ion propagation, which resulted in the description of the Bragg peak and the energy spectrum of secondary electrons [10,11]. The practical goal of these works provided a recipe for an economical calculation of the Bragg peak position and shape. It was concluded theoretically that the cross section of ionization of molecules of the medium, singly differentiated with respect to the energies of secondary electrons, is the most important physical input on this scale (the longest in distance and highest in energy). Relativistic effects play an important role in describing the position of the Bragg peak as well as the excitation channel in inelastic interactions [10]. The effect of charge transfer and projectile scattering influence the shape of the Bragg peak [10]. The effects of nuclear fragmentation happening in the events of projectile collisions with the nuclei of the medium are also important on this scale.

The next scale in energy and space is related to the transport of the secondary particles, which has been considered in Refs. [7,12], but it may still be revisited. The results of these analyses give the spatial distributions of secondary particles as well as an accurate radial dose distribution.

The goal of the analysis of DNA damage mechanisms is to obtain the effective cross sections for the dominant processes, which should be taken into account in order to calculate the probability of different lesions caused by different effects. The above three stages of processes represent not only different spatial scales, but also different time scales, ranging from 10^{-21} to 10^{-5} s. The aim of the physical part of the analysis is the calculation of the spatial distribution of primary DNA damage, including the degree of complexity of this damage. Then the repair and other biological effects can be included and thus the relative biological effectiveness (RBE) can be calculated. The RBE [1,5] is one of the key integral characteristics of the effect of ions compared to that of photons. This ratio compares the doses of different projectiles leading to the same biological effect.

Traditionally, the radial dose, calculated in Ref. [12], is related to the radial distribution of damage. However, this does not include the complexity of damage, which may not be directly related to the dose. It is still not clear how to relate the dose to the complexity of the damage. This work is a step in this direction.

Finally, the analysis of the possibility of thermomechanical damage pathways was presented in Ref. [10] and was further advanced in Refs. [13,14]. It was shown that forces, caused by high-pressure gradients emerging as a result of local heating of the medium by passing ions, can be strong enough to break covalent bonds (more than 10 nN), but act only for a very short time.

This work is devoted to the calculation of damage complexity and its distribution. This is an important stage in the multiscale approach since it is closely related to the

[*]On leave from A. F. Ioffe Physical Technical Institute, Division of Solid State Electronics, St. Petersburg 194021, Russia.

probability of cell death as a result of damage [15–19]. Damage complexity is one of the defining factors in calculating the RBE.

In Sec. II we define the complex damage and present a way to quantify it. In Sec. II A we calculate the fluence of secondary electrons as a step in the assessment of complex damage. In Sec. II B we calculate the radial dose distribution and give an example of a calculation of the complex damage on that basis.

II. DISTRIBUTION OF THE COMPLEX DAMAGE

Complex damage is defined as the number of DNA lesions, such as double-strand breaks (DSBs), single-strand breaks, abasic sites, and damaged bases, that occur within about two helical turns of a DNA molecule so that when repair mechanisms are engaged they treat a cluster of several of these lesions as a single damage site [15–17]. In Ref. [9] the complexity of DNA damage has been quantified by defining a cluster of damage as a damaged portion of a DNA molecule by several independent agents such as secondary electrons, holes, or radicals.

In humans, DNA molecules are by and large located in cell nuclei, where they are organized with proteins into chromatin fibers. The main structural unit of chromatin fibers is a nucleosome [20]. A nucleosome core particle consists of about a 146-base-pair section of a DNA molecule wrapped around a cylindrical aggregate of eight histone proteins (histone octamer).

A. Damage complexity distribution from the random-walk approach

In Ref. [7] we studied the transport of secondary electrons to a given DNA convolution. This study led to the calculation of the radial distribution of DSBs with respect to the ion path. This calculation was limited by only considering secondary electrons to be the agents of DNA lesions. Nevertheless, this allowed us to make an estimation of the number of DSBs produced by ions per unit length of path in the vicinity of the Bragg peak. The results obtained in that work were in reasonable agreement with the experimental data [21]. The approach of Ref. [7] can be used for calculating the radial distribution of damage complexity.

Let us choose two adjacent convolutions of a DNA molecule as a target. Then the average number of lesions per this segment of DNA, N, is given by the product of the probability of inducing damage by a secondary particle on impact Γ by the fluence through the target. Alternatively, it is given by the same probability multiplied by the volume of the segment and by the number density of agents. The probability of complex damage is then a Poisson distribution $P(N,\nu)$,

$$P(\rho,\nu) = \exp[-N(\rho)]\frac{N(\rho)^{\nu}}{\nu!}, \tag{1}$$

where ν is the degree of complexity [9]. In Eq. (1), N is written as a function of ρ, the distance of the segment from the path. Our goal is to calculate the radial distribution of complex damage with respect to the ion path in the simplest case, when all agents are equivalent, keeping the probability Γ as a parameter. In this paper we limit secondary particles to secondary electrons. A further development will include transport of secondary particles including chemical reactions and more details of their distributions.

In this section we calculate the fluence of the secondary electrons through the DNA segment. In order to do this we consider their diffusion from the place of their origin, as done in Ref. [7]. We assume that the diffusion of the secondary electrons is cylindrically symmetric with respect to the ion's path and calculate the number of electrons that hit two adjacent convolutions of a DNA molecule. The cylindrical diffusion in the vicinity of the Bragg peak can be justified by the fact that during the time that it takes secondary electrons to diffuse by about 10 nm, the projectile moves a distance of about 1 μm [14]. The linear energy transfer (LET) along this distance, described by the coordinate ζ, remains nearly constant, as does the production of secondary particles per unit length $\frac{dN}{d\zeta}$; therefore, the latter is independent of ζ. This number of secondary electrons produced per nanometer of the ion's path is taken to be equal to 20, which corresponds to the average number of ionizations per nanometer of the ion's path in the vicinity of the Bragg peak [7,10].

Naturally, we expect the largest damage to occur when the incident ion passes through a nucleosome. Therefore, in this paper we calculate the complex damage that takes place in two consecutive convolutions of a DNA molecule on the surface of a nucleosome situated outside the ion's path (neglecting the stretches of linker DNA connecting nucleosomes). In what follows, a nucleosome is represented by a cylinder with a radius of 5.75 nm and height of 6 nm and the target section of a DNA molecule is a rectangular patch (7.2×2.3 nm^2) of its surface, as shown in Fig. 1.

In order to calculate the fluence we consider the rate of secondary electrons, dN_A/dt, at the time t, passing through the patch $d\mathbf{A}$, located at a distance ρ from the path. According to Ref. [22], for a cylindrically symmetric random walk, it is given by the expression

$$\begin{aligned}\frac{dN_A(\mathbf{r},t)}{dt} &= d\mathbf{A}\cdot D\nabla P(t,\rho)\frac{dN}{d\zeta}\\ &= d\mathbf{A}\cdot D\mathbf{n}_{\rho}\frac{\partial P(t,\rho)}{\partial\rho}\frac{dN}{d\zeta},\end{aligned} \tag{2}$$

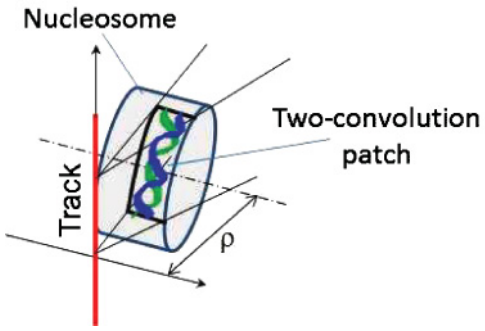

FIG. 1. (Color online) Geometry of the problem. Secondary electrons radially diffuse from the ion's path and interact with a section of DNA molecule wrapped around a histone octamer.

where $D = \bar{v}l/4$ is the diffusion coefficient, l is the elastic mean free path of electrons in the medium,[1] $\bar{v}$ is the speed of the electron, $\mathbf{n}_\rho$ is a unit vector in the radial direction from the path, and

$$P(t,\rho) = \frac{1}{\pi \bar{v} t l} \exp\left(-\frac{\rho^2}{\bar{v} t l}\right) \tag{3}$$

is the probability density to observe a randomly walking electron at a time t and a distance ρ from the path. Eventually we are going to integrate Eq. (2) over both the time (to get the total number of electrons incident on the patch $d\mathbf{A}$) and $d\mathbf{A}$ (in order to calculate the total number of electrons incident on a two-twist segment of a DNA molecule). Before we do this, we need to somewhat modify Eqs. (2) and (3).

First, the time dependence can be translated to the dependence on the number of steps, k, using $\bar{v}t = kl$ and $\bar{v}dt = ldk$. Second, there is a probability that the electron interacts with a molecule inelastically, loses energy, and drops off from a random walk. In order to account for such a subtraction, we introduce an attenuation factor $\epsilon(k)$. In Ref. [7] we used

$$\epsilon(k) = \gamma \exp(-\gamma k), \tag{4}$$

where γ is a constant that is proportional to the ratio of mean free paths between inelastic and elastic collisions. This expression is physically motivated, but it does not take into account the energy dependence of mean free paths and their ratio. In this paper we will keep the elastic mean free path l energy independent and equal to 1 nm [12], while we will use the attenuation given by

$$\epsilon(k) = \exp\left[\alpha \exp\left(-k^\beta\right)\right]. \tag{5}$$

This expression with constants $\alpha = 60$ and $\beta = 0.055$ appears as a result of fitting the radial dose distribution derived from a model of secondary electron transport to that obtained using Monte Carlo simulations [23]. This model assumes a random walk of electrons with a constant mean free path, i.e., the same used by us in this section. Equation (5), with a modified dependence on k, implicitly introduces the dependence of the attenuation on energy. The attenuation according Eq. (5) is steeper than that according to Eq. (4) for small k. This means that electrons with higher energy tend to lose it in inelastic collisions more quickly than those with smaller energies and the attenuation at large k is much smaller. We will return to this parametrization in Sec. II B.

Now we can rewrite Eq. (2), substituting Eq. (3), including the attenuation, and switching from variable t to k as

$$dN_A(\mathbf{r},k) = dk\, d\mathbf{A} \cdot \mathbf{n}_\rho \frac{\rho}{2\pi k^2 l^2} \exp\left(-\frac{\rho^2}{kl^2}\right) \epsilon(k) \frac{dN}{d\zeta}, \tag{6}$$

and integrate it over the target part of the surface of the cylinder, representing a nucleosome. The results of integration [Eq. (6)] over time and the area of the patch are shown in Fig. 2. As expected, this number decreases with distance ρ from the path.

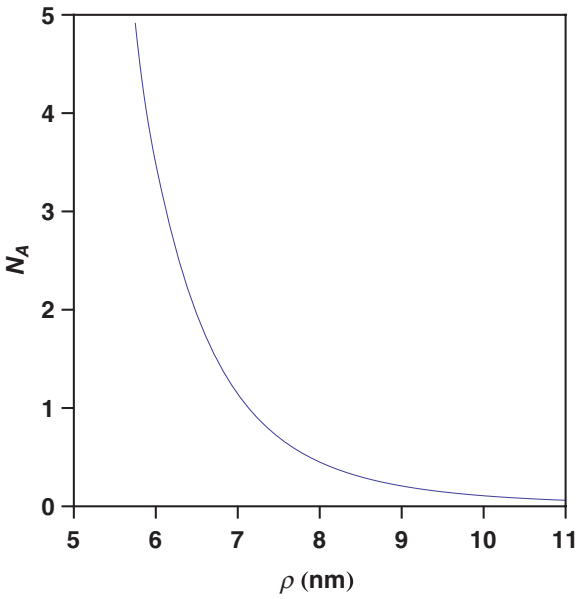

FIG. 2. (Color online) Number of secondary electrons diffused through a two-convolution segment of DNA molecule on the surface of a nucleosome in the vicinity of the ion's path, plotted as a function of the distance ρ of the nucleosome from the path. The calculation is done using the attenuation function given by Eq. (5).

If we multiply this number N_A by the probability Γ of producing a lesion in a DNA molecule, uniformly distributed on the surface of the nucleosome, we obtain the dependence of the number of lesions on the distance from the path. Then Eq. (1) can be used, with

$$N(\rho) = \Gamma N_A(\rho), \tag{7}$$

to calculate the radial distributions of probabilities of clusters of lesions.

This number has to be corrected to include further ionizations and holes, which also play a role in the damage. Holes may recombine producing Auger electrons, capable of inducing lesions to DNA [24]. Before these corrections are made, these calculations remain qualitative. When the transport properties of electrons and other secondary particles in the medium are known and $N(\rho)$ is calculated more definitely, the approach to the calculation of the clustered damage, described above, can be useful.

In addition to this calculation, it is possible to compute similar probabilities for cases when the path passes through the nucleosome; however, this would require calculating the transport of secondary electrons through a histone and knowledge of the elastic and inelastic cross sections of electrons in this medium. Recent calculations indicate a 20% higher stopping power of DNA compared to liquid water [25]. We will defer these calculations until another time. However, it may be worth mentioning that the clustered damage of a histone may also deserve attention in regard to cell damage.

The calculation of the number of secondary electrons passing through a patch on a nucleosome presented in this section is important for several reasons. First, it can be compared with Monte Carlo simulations done for the purposes of nanodosimetry [26]. Second, it will be possible to compare

[1] In two dimensions, l is a product of the mean free path in three dimensions multiplied by the factor of $\sqrt{2/3}$.

this dependence (correspondingly modified) with dosimetric experiments [27,28]. At this point it is possible to use the dependence shown in Fig. 2 for the calculation of the complex damage (using additional parameters); however, in this paper we choose to use the radial dose distribution to demonstrate a calculation of complex damage. At this moment, the latter approach allows for more checkpoints and we describe it in the following section.

B. Derivation of damage complexity from the radial dose distribution

As shown in Ref. [12], the radial number density distribution of secondary electrons that lose energy and become thermalized or bound is related to the radial dose. Here we revisit the calculation of the radial dose and infer the secondary particle distribution, with the complexity distribution following from that.

Let us assume that all secondary electrons start from the ion's path and propagate via a random walk in two dimensions; this corresponds to the cylindrically symmetric propagation (neglecting some fast δ electrons). Then, according to Eq. (3), rewritten in terms of k, the probability to find a secondary particle in a cylindrical layer of unit length between ρ and $\rho + d\rho$ after k random steps is $\frac{dN_s}{d\zeta} P(k,\rho) 2\pi\ \rho\, d\rho$. This probability is normalized to $\frac{dN_s}{d\zeta}$ for any number of steps k if we integrate over $d\rho$ from 0 to infinity. The normalization does not change if we include the attenuation $\epsilon(k)$ due to inelastic processes and introduce a distribution over k. Transferring from the sum to the integral, which is appropriate for large k, this can be written as

$$\int_1^\infty \int_0^\infty P(k,\rho)\epsilon(k) 2\pi\ \rho\, d\rho\, dk = 1. \tag{8}$$

Then the density of the particles, which lost energy within the cylindrical layer of a unit length between ρ and $\rho + d\rho$, can be obtained by dividing the integrand of Eq. (8) by the volume of this shell of a unit length, i.e., $2\pi\ \rho\, d\rho$, and the radial dose $\mathcal{D}(\rho)$ can be obtained by multiplication of this density by the average energy per particle $\bar{W} = 45$ eV [10]:

$$\mathcal{D}(\rho) = \bar{W} \frac{dN_s}{d\zeta} \int_1^\infty P(k,\rho)\epsilon(k) dk. \tag{9}$$

This dose is normalized by the LET $\mathcal{L}$:

$$\int_0^\infty \mathcal{D}(\rho) 2\pi\ \rho\, d\rho = \mathcal{L}. \tag{10}$$

However, the radial dose distribution calculated using Eq. (9) with the attenuation, defined by Eq. (4), does not agree with simulations of, e.g., Ref. [23]. The reason for this is that in Eq. (4) we have assumed energy-independent attenuation. According to, e.g., Ref. [29], both elastic and inelastic mean free paths are energy dependent. Moreover, as pointed out in Ref. [7], the dependence of ranges of low-energy electrons in liquid water on energy, discussed in Ref. [30], indicates that the attenuation steeply decreases as the energy of the electron decreases (after several inelastic collisions). This can be taken into account by parametrizing the attenuation as a function of k so that the dose calculated using Eq. (9) agrees with experiments and simulations. In this work we have found that

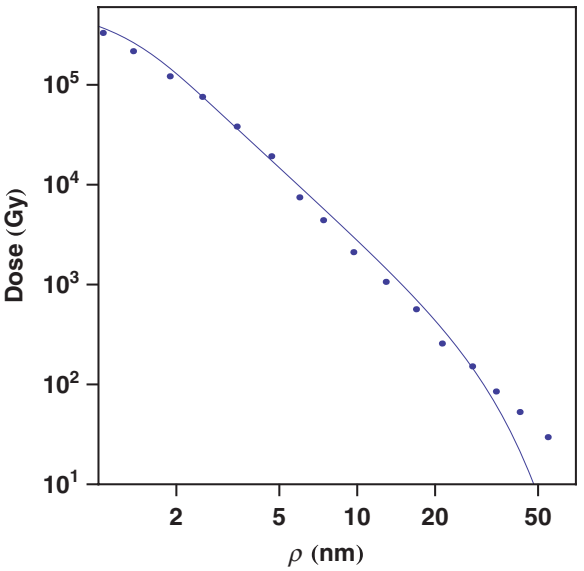

FIG. 3. (Color online) Comparison of the calculated radial dose (line) [Eq. (9)] with that simulated in Ref. [23] (dots) for 25-MeV/nucleon carbon ions.

the dose calculated using Eq. (9) with attenuation defined by Eq. (5) with parameters α and β given above[2] is in reasonable agreement with that simulated in Ref. [23]. This comparison is shown in Fig. 3.

The simulation done in Ref. [23] corresponds to 25-MeV/nucleon carbon ions with $\mathcal{L} = 60$ eV/nm. This is about 4 mm in front of the Bragg peak, where $\mathcal{L} = 900$ eV/nm. Therefore, we recalculated the same dose using the procedure described above for 0.3-MeV/nucleon carbon ions with $\mathcal{L} = 900$ eV/nm. The result is presented in Fig. 4. This distribution can be compared to the experimental measurements of the

[2]Equation (5) has to be divided by $\int \epsilon(k) dk$ for normalization.

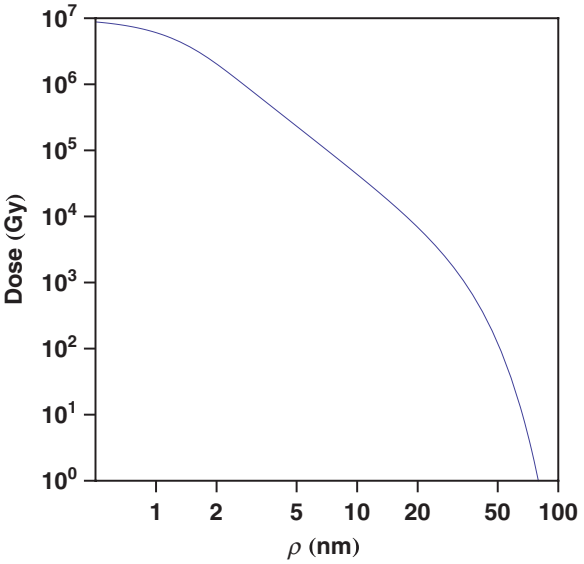

FIG. 4. (Color online) Calculated radial dose distribution for a LET of 0.9 keV/nm.

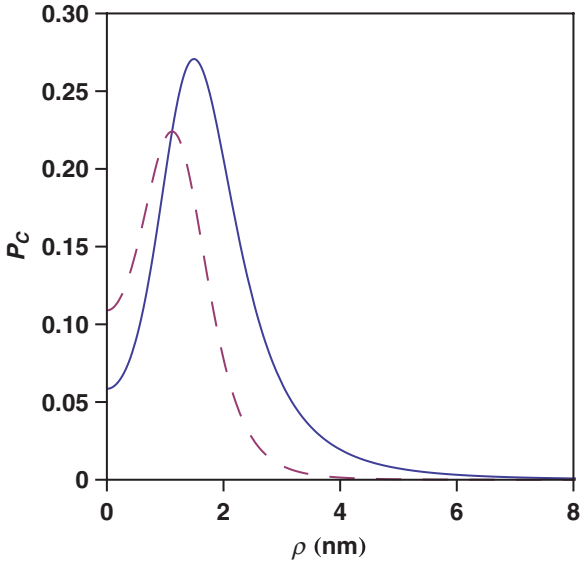

FIG. 5. (Color online) Radial distribution of clusters of two lesions (solid line) and clusters of three lesions (dashed line) for $\Gamma = 0.1$.

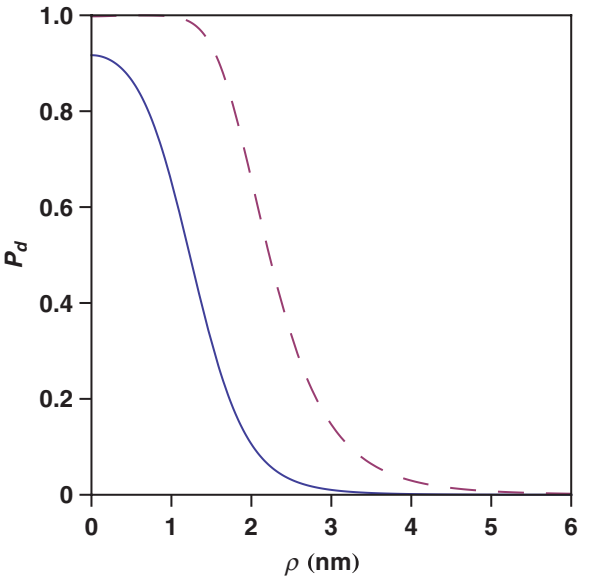

FIG. 6. (Color online) Radial distribution of clusters of three and more lesions, deemed proportional to the probability of cell death. The solid curve corresponds to $\Gamma = 0.1$ and the dashed curve corresponds to $\Gamma = 0.3$.

radial dose distribution; however, such data are currently unavailable for such a LET.

Using this dose distribution around a single ion's path, we can calculate the distribution of clusters of DNA damage. In order to do this, we have to divide the expression in Eq. (9) for the dose by $\bar{W}$ and obtain the radial distribution of the density of inelastically interacting secondary electrons. If we then multiply that by the effective volume of the target segment DNA and the probability of producing a lesion Γ, we will obtain $N(\rho)$. Then we can calculate the radial distribution of complex damage using Eq. (1). This will be correct only if $N(\rho)$ does not significantly change over this volume.

If we assume that the effects of varying $N(\rho)$ on the size of some effective volume can be neglected, then we can calculate the radial distribution P_c of clusters for a given ν. An example of such dependences for a volume of 40 nm^3 (corresponding to the volume occupied by two convolutions of DNA molecule) and $\Gamma = 0.1$ of two- and three-lesion clusters is shown in Fig. 5.

These distributions give us an opportunity to verify the significance of clustering. If, e.g., all clusters containing three or more lesions are lethal for the cell, we can add up their probabilities and plot the dependence of the probability of cell death P_d on the distance from the path. These dependences for $\Gamma = 0.1$ and 0.3 are shown in Fig. 6. This figure indicates that if the clusters of three and more lesions per nucleosome are indeed lethal, then the effective distance from the path on which the cells are killed is less than 1.5 nm for $\Gamma = 0.1$ and exceeds 2 nm for $\Gamma = 0.3$. Hence, in the former case, it is essential that the ion passes through a nucleosome in order to kill the cell, while in the latter, a nucleosome can be at a distance and still be severely damaged. This analysis opens several fields for comparison with experiments: the dependence of lethality on the radial distance from the path and on the size of clusters of lesions for biophysics and the radial dependence of the dose and cluster damage distribution for nanodosimetry. The radial scale in Fig. 6 is shorter than 10 nm. Even though this size is about 1000 times smaller (for glial cells) than that of the cell's nucleus [7], it plays a significant role in calculations of the probability of cell death and will be critical for the comparisons with nanodosimetric data [26–28,31].

If we keep the assumption that three- and higher-order lesion clusters are lethal to the cell, then we can plot the dependence of $1 - P_d$, which is similar to the probability of cell survival, on the radial dose. This dependence is presented in Fig. 7 and can also be compared with experiments. The scale on the abscissa for the radial dose is indeed in MGy.

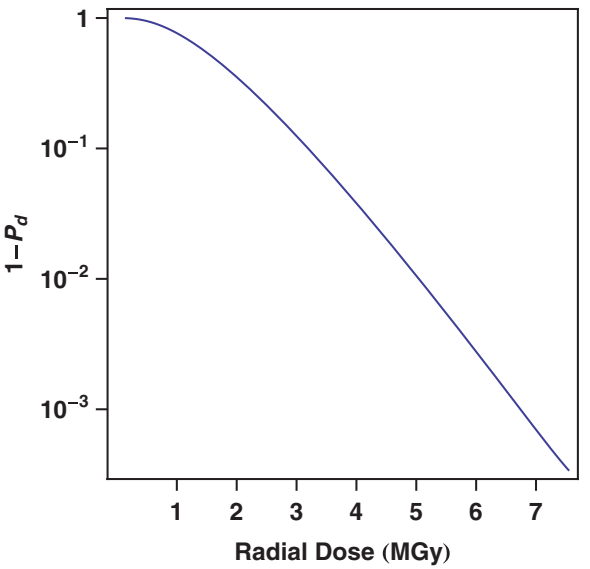

FIG. 7. (Color online) Dependence of $1 - P_d$, which is similar to the cell survival rate (dimensionless), on the local radial dose per ion with $\Gamma = 0.3$.

This is larger (by a factor of 10^6) than that in typical cell survival curves [32], where the dose is absolute, i.e., planar integrated per ion and distributed for the whole beam. A typical spatial distance between the ion paths is larger than 350 nm.[3] Therefore, the volume per 1 nm of the ion's path is at least 10^5 nm^3. This makes the average integral dose at the Bragg peak of a single carbon ion about 7×10^{-3} eV nm^{-3} = 110 Gy. This dose has to be averaged once again when one considers the whole ion beam. This results in another factor of the order of 0.1, which reduces the maximum dose to 10–15 Gy. The absolute dose is important for treatment planning, but here we are interested in a more detailed description and the radial, not averaged, dose is more relevant for this purpose. This is why we present the dependence of a probability cell survival on the local radial dose. Below we show how to do a planar integration and give an example of an estimate.

The radial distributions of clustered damage probabilities can be integrated over the radius in order to obtain the probability of lethal damage per unit length. This is relevant for current experiments. When experimentalists study foci that reveal the efforts of proteins to fix damaged DNA they observe that the foci are very large compared to the scale of the radial distribution of the dose. The experimentalists can measure the linear density of clusters along the path and hypothesize about the number of certain lesions, such as DSBs, per unit length [33].

In order to obtain the longitudinal distributions of clusters, we have to introduce the density of the distribution of nucleosomes with respect to the ion path $\eta(\rho)$. We can then integrate the radial-dependent probability of the complex damage given by Eq. (1) [for appropriate $N(\rho)$ dependence] with this density distribution:

$$P(\nu) = \int_0^\infty \exp\left[-N(\rho)\right] \frac{N(\rho)^\nu}{\nu!} \eta(\rho) 2\pi\, \rho\, d\rho. \qquad (11)$$

This gives the number of clusters of ν lesions per nanometer, which can be compared with the nanodosimetric experiments [26–28,31] and can give still another relation for unknown parameters such as Γ and the dependence of the lethality of damage on the order of cluster ν.

[3] According to the beam data [1].

The density of the distribution of nucleosomes $\eta(\rho)$ depends on the structure of packing nucleosomes in fibers. If we consider a section of a cylindrical fiber of tightly packed nucleosomes [20] to be parallel to the path 1 nm away from its surface, then an estimate made with the above assumptions producing the maximal effect of damage complexity predicts about three complex damage sites (with $\nu > 2$) per 10 nm of a carbon ion's path.

III. CONCLUSION

The multiscale approach was designed in order to understand the mechanisms that make the ion-beam therapy effective. This includes an understanding of what is truly different between different therapies. It is widely accepted that the high-LET radiation brings about a high dose in the desired location. However, it is not yet clear whether the dose entirely accounts for all biological consequences, namely, how different the dose and complexity distributions are and which of them is responsible for the cell death. This paper tackled these questions and, although more experiments are needed to confirm them, the principle framework of the problem has been set up.

The main accomplishments of this paper are the calculation of the radial dose distribution (comparable with that obtained by simulations), the derivation of the radial distribution of secondary electrons from the radial dose distribution, and the calculation of the radial distributions of different clusters of lesions. On the basis of these distributions we developed models for calculations of dependences of the probabilities of cell death as a result of complex damage of DNA at a distance from the ion's path and along the path. These calculations may be very practical and we hope that they will be explored by experimentalists in nanodosimetry as well as by biophysicists. The main point in our approach to damage complexity is that it can be described by a spatial distribution and compared to the radial dose distribution and the distribution of killed cells.

ACKNOWLEDGMENTS

We are grateful for the support of the authors' collaboration by COST Action MP1002 "Nano-scale insights in ion beam cancer therapy." E.S. thanks J. S. Payson for a constructive critique.

[1] U. Amaldi and G. Kraft, J. Radiat. Res. **48**, A27 (2007).
[2] H. Tsujii *et al.*, New J. Phys. **10**, 075009 (2008).
[3] E. Fokas, G. Kraft, H. An, and R. Engenhart-Cabillic, Biochimica et Biophysica Acta **1796**, 216 (2009).
[4] D. Schardt, T. Elsässer, and D. Schulz-Ertner, Rev. Mod. Phys. **82**, 383 (2010).
[5] M. Durante and J. Loeffler, Nature Rev. Clin. Oncol. **7**, 37 (2010).
[6] I. Baccarelli, F. Gianturco, E. Scifoni, A. V. Solov'yov, and E. Surdutovich, Eur. Phys. J. D **60**, 1 (2010).
[7] A. V. Solov'yov, E. Surdutovich, E. Scifoni, I. Mishustin, and W. Greiner, Phys. Rev. E **79**, 011909 (2009).
[8] E. Surdutovich, E. Scifoni, and A. V. Solov'yov, Mutat. Res. **704**, 206 (2010).
[9] E. Surdutovich, A. V. Yakubovich, and A. V. Solov'yov, Eur. Phys. J. D **60**, 101 (2010).
[10] E. Surdutovich, O. I. Obolensky, E. Scifoni, I. Pshenichnov, I. Mishustin, A. V. Solov'yov, and W. Greiner, Eur. Phys. J. D **51**, 63 (2009).
[11] E. Scifoni, E. Surdutovich, and A. V. Solov'yov, Phys Rev. E **81**, 021903 (2010).
[12] E. Scifoni, E. Surdutovich, and A. V. Solov'yov, Eur. Phys. J. D **60**, 115 (2010).

[13] M. Toulemonde, E. Surdutovich, and A. V. Solov'yov, Phys. Rev. E **80**, 031913 (2009).
[14] E. Surdutovich and A. V. Solov'yov, Phys. Rev. E **82**, 051915 (2010).
[15] S. Malyarchuk, R. Castore, and L. Harrison, DNA Repair **8**, 1343 (2009).
[16] S. Malyarchuk, R. Castore, and L. Harrison, Nucleic Acids Res. **36**, 4872 (2008).
[17] E. Sage and L. Harrison, Mutation Research **711**, 123 (2011).
[18] J. Ward, Prog. Nucleic Acid Res. Mol. Biol. **35**, 95 (1988).
[19] J. Ward, Radiat. Res. **142**, 362 (1995).
[20] M. Depken and H. Schiessel, Biophys. J. **96**, 777 (2009).
[21] B. Jakob, M. Scholz, and G. Taucher-Scholz, Radiat. Res. **159**, 676 (2003).
[22] S. Chandrasekhar, Rev. Mod. Phys. **15**, 1 (1943).
[23] I. Plante and F. Cucinotta, Radiat. Environ. Biophys. **49**, 5 (2010).
[24] E. Surdutovich and A. V. Solov'yov, Phys. Rev. Lett. (submitted for publication).
[25] I. Abril, R. Garcia-Molina, C. Denton, I. Kyriakou, and D. Emfietzoglou, Radiat. Res. **175**, 247 (2011).
[26] M. Bug, E. Gargioni, S. Guatelli, S. Incerti, H. Rabus, R. Schulte, and A. Rosenfeld, Eur. Phys. J. D **60**, 85 (2010).
[27] E. Fuks, Y. Horowitz, A. Horowitz, L. Oster, S. Marino, M. Rainer, A. Rosenfeld, and H. Datz, Radiat. Prot. Dosimetry **143**, 416 (2011).
[28] V. L. Pisacane, Q. E. Dolecek, H. Malak, F. A. Cucinotta, M. Zaider, A. B. Rosenfeld, A. Rusek, M. Sivertz, and J. F. Dicello, Radiat. Prot. Dosimetry **143**, 398 (2010).
[29] C. Tung, T. Chao, H. Hsieh, and W. Chan, Nucl. Instrum. Methods Phys. Res. Sect. B **262**, 231 (2007).
[30] J. Meesungnoen, J.-P. Jay-Gerin, A. Filali-Mouhim, and S. Mankhetkorn, Radiat. Res. **158**, 657 (2002).
[31] B. Cassie, A. Wroe, H. Kooy, N. Depauw, J. Flanz, H. Paganetti, and A. Rosenfeld, Med. Phys. **37**, 311 (2010).
[32] M. Krämer, Nucl. Instrum. Methods Phys. Res. Sect. B **267**, 989 (2009).
[33] F. Tobias, M. Durante, G. Taucher-Scholz, and B. Jakob, Mutat. Res. **704**, 54 (2010).